Cross-sectional shape effects on the electronic properties of Silicon nanowires

Redwan Noor Sajjad, Sishir Bhowmick and Quazi D. M. Khosru

***Abstract*—The electronic properties of Silicon nanowires are studied using empirical tight binding $sp^3d^5s^*$ model for three different cross-sectional shapes - square, circular and triangular. For two different growth directions <100> and <110>, it is observed that the electron effective masses at the Γ point is lowest for triangular wire. The conduction band valley splitting at the Γ point for <100> wire is higher for triangular wire compared to the other two shapes. The valence bands are more degenerate for circular wire than the other two and their splitting is highest for square wire. Hole effective mass at the valence band maxima for <100> wire is significantly lower for triangular wire than that of the other two shapes which show large increase in hole effective mass as a result of quantum confinement. These electronic properties are compared against same cross-section area which is varied from $0 - 30nm^2$. The energy band gap shows no variation due to wire shape. It only depends on cross-section area. Variations in the electronic properties due to shape diminish gradually as cross-sectional area is increased.**

***Index Terms*—Silicon Nanowires (SiNWs), cross-sectional shape.**

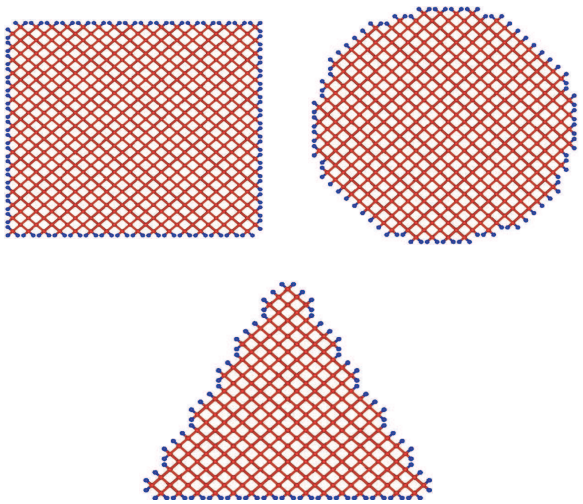

Fig. 1. <100> Silicon nanowires with different cross-sectional shapes - Square, Circular and Triangular.

I. Introduction

There has been aggressive downscaling of conventional transistors in the past few years by reducing gate length, oxide thickness and channel depth. Performance degradation takes place due to this scaling including short channel effects, reduced electron mobility and weakened gate control. For future nanotechnology, novel materials such as nanowires can be attractive building blocks because of their superior characteristics. The controlled growth of silicon nanowires (SiNWs), their applications as field effect transistors and logic circuits have been demonstrated experimentally [1]–[4]. The Silicon Nanowire Field Effect Transistors (SiNWFET) with gate all around structure show excellent gate control and current drive and they are also compatible with CMOS processes.

As the nanowires' dimension is in the nanometer regime, effects like tunneling and quantum confinement play dominant role.There have been numerous simulation works on Silicon nanowires in recent times. The electronic properties of SiNWs has been studied using atomic orbital basis with empirical tight-binding parameters [5]–[7] and also using first principle calculations [8]–[10]. At the device level, nanowire transistor current has been calculated using bulk effective masses [11], [12], nanowire confined masses [12]–[14] and full band simulation [15].

Redwan Noor Sajjad, Sishir Bhowmick and Quazi D. M. Khosru are with the Department of Electrical and Electronic Engineering, Bangladesh University of Engineering and Technology, Dhaka-1000, Bangladesh (email: redwan@eee.buet.ac.bd).

Nanowire of different orientations and shapes have been studied by several experimental groups [4], [16]. Square [11], [12] and circular [6] cross-sections are the most frequently used shapes for simulations. We also find first principle calculations for pentagonal and hexagonal nanowires [17], [18]. In this paper, Silicon nanowires are simulated using the $sp^3d^5s^*$ model to observe the effects of different cross-sectional shapes. Calculations show that the conduction and valence band degeneracy and also the effective masses change with wire shape.

II. Approach

The SiNWs used in this study are grown in <100> and <110> directions. The cross section of <100> SiNWs of all shapes (square, circular and triangular)are shown in Fig. 1. The nanowire growth direction is x, which is into (or out of) the paper. The y and z directions are <010> and <001>. The cross section looks rectangular. The unit cell is 0.543 nm long and has 4 atomic layers. For growing circular or triangular wires, a square nanowire is grown first. Then the outer atoms are eliminated to form the desired shape. The open bonds at the wire boundaries are passivated using hydrozen.

For band structure calculation, the Hamiltonian is created as

$$H(k_x) = H_0(k_x) + t_{01}e^{ikx\triangle x} + t_{10}e^{-ikx\triangle x} \quad (1)$$

Here k_x is the one dimensional (1D) wave vector and $\triangle$ x is the distance between the last layer of a unit cell and the first

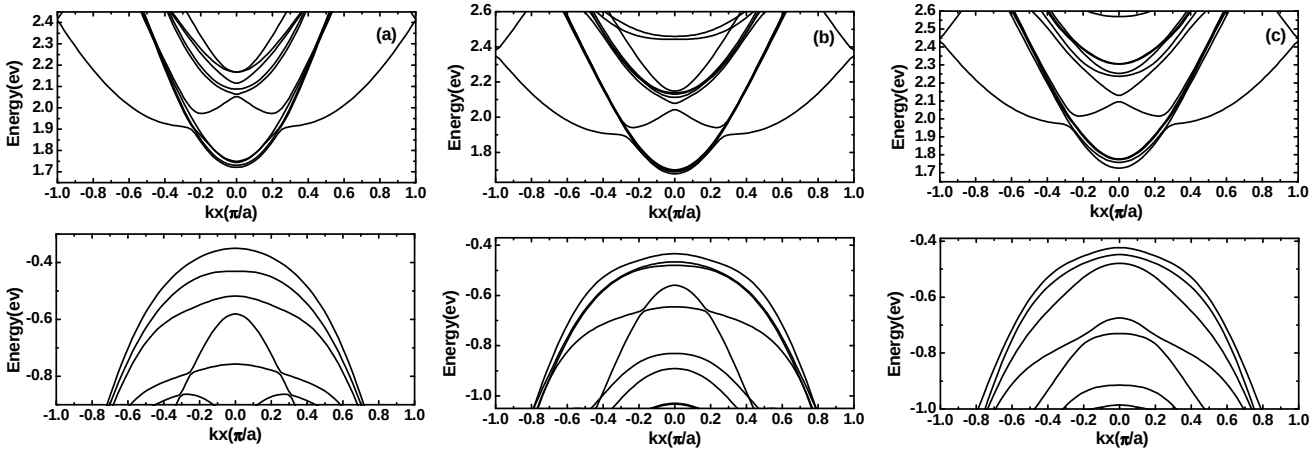

Fig. 2. The bandstructure of <100> SiNWs with (a) square, (b) Circular, (c) Triangular cross-section

layer of the next unit cell. The matrix elements of $H_0(k)$ are created from

$$H_0(i,j) =< \phi_{i,n}|H|\phi_{j,m} > e^{ik_x(x_m - x_n)} \tag{2}$$

and those of t_{01} are created from

$$t_{01}(p,q) =< \phi_{p,u}|H|\phi_{q,v} > \tag{3}$$

Here n and m label the atoms in the same unit cell, and u and v label the atoms between adjacent unit cells. The basis ϕ, is the $sp^3d^5s^*$ atomic orbitals and $\phi_{i,n}$ is the i^{th} orbital of the n^{th} atom. The tight-binding parameters are taken from Boykin [19] and Zheng [20] and the energy integral expressions are taken from Slater [21]. The band structure is obtained by calculating the eigen energies of H_{kx} defined in Eq. 1. Finite difference method is employed to calculate effective mass,

$$\frac{1}{m^*} = \frac{1}{\hbar^2}\frac{\partial^2 E}{\partial k_x^2} = \frac{1}{\hbar^2}\frac{E_- - 2E_0 + E_+}{(\triangle k_x)^2} \tag{4}$$

where E_0 is the energy at the desired value of k where we want to calculate m^* and E_+ and E_- are the energies at $k \pm \triangle k_x$ respectively. We use a $\triangle k_x$ value of $(0.001) \times \pi/a$. In this paper, we use the term dimension to imply length of one side when the cross-section is square, diameter for circular and length of one arm for triangular nanowire. In Fig. 1, D=4.38nm.

III. Numerical Results and Discussions

Fig. 2 shows the bandstructure for a <100> oriented Silicon nanowire for three different shapes for same cross-section area ($2.70nm^2$). The bulk Silicon is an indirect bandgap material having conduction band minimum at 0.832 $\times$ 2π/a in the Δ direction. It has six equivalent Δ valleys. The nanowire is a direct band gap material. For nanowire grown in <100> direction, four of the six equivalent Δ valleys are projected at Γ point in the one dimensional Brilluoin zone forming the conduction band minimum. The other two valleys are zone folded to $\pm$0.36 $\times$ π/a in the wire Brilluoin zone. The four valleys are degenerate at the Γ point. For <110> wires, two of the bulk valleys are projected at the Γ point and the other valleys are found at $\pm 0.81 \times \pi/a$.

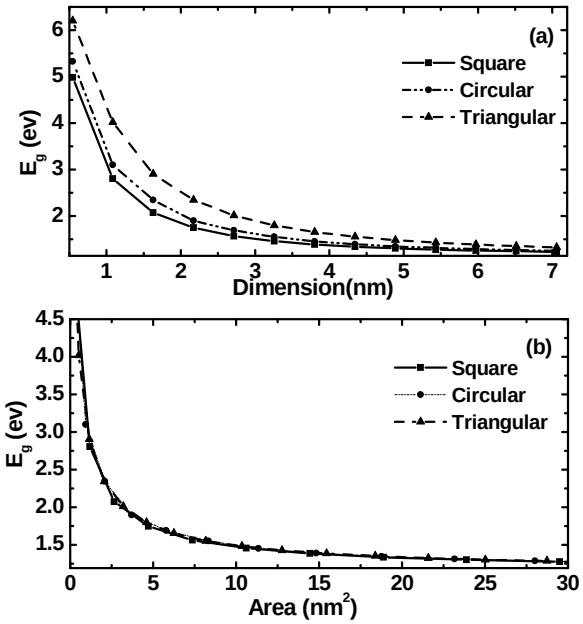

Fig. 3. Bandgap variation with (a) dimension, (b) cross-section area.

Fig. 3(a) shows the variation of band gap with dimension. The band gap increases with decreasing cross-section area as a result of quantum confinement. For large wires, the bandgap equals that of bulk Silicon (1.13ev). When plotted against dimension, square nanowires exhibit lowest bandgaps and the bandgap for the triangular wire is the highest. But this dissimilarity is not for wire shape, because the triangular wire with dimension D has an area of $0.433D^2$, which is 43.3% of the square wire area (D^2) having the same dimension D. This fact is clear when we plot the bandgap against cross-section area, the bandgap for all shapes are remarkably similar (Fig. 3 (b)). This reveals that the energy gap simply depends on the wire cross-section area, not on the shape.

The conduction band degeneracy at the Γ point for <100> wire is considered next (Fig. 4 (a)). The forth highest band is plotted taking the lowest conduction band as reference. The four valley degeneracy is almost similar for square and circular

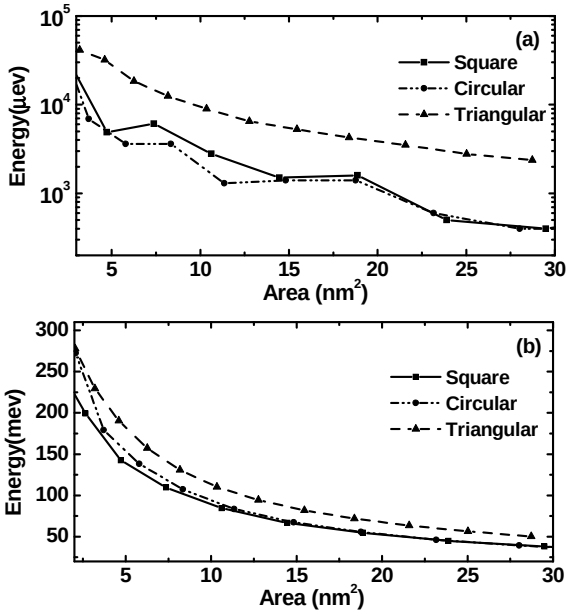

Fig. 4. Effect of wire cross-section area on Δ_4 and Δ_2 conduction band valleys, (a) Variation of forth highest conduction band energy at Δ_4 valley taking the lowest energy as reference, (b) Splitting of Δ_4 and Δ_2 valleys.

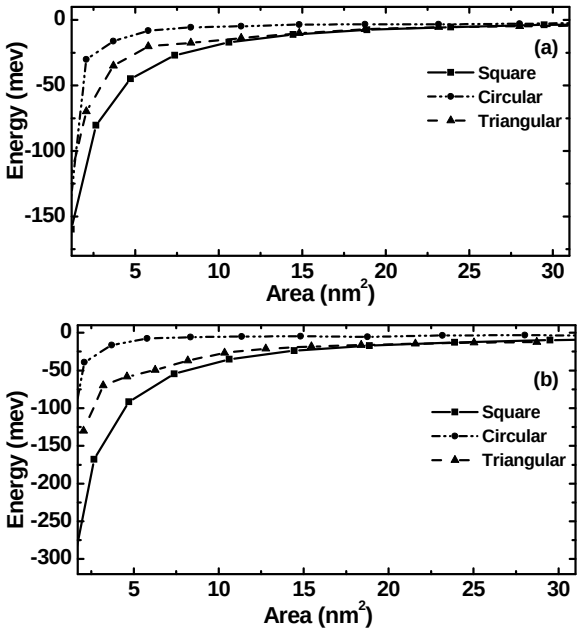

Fig. 5. Effect of wire area on the splitting of the three highest valence bands taking the highest valence band Ev_1 as reference, (a) The energies Ev_2 and (b) Ev_3 with respect to Ev_1.

wires, while the valleys are less degenerate for triangular wire. As the cross-section area is increased, the separation between Δ_4 and Δ_2 valley energies is decreased (Fig. 4 (b)). This energy difference is lowest for square wire and highest for triangular wire. Fig. 5 shows the effect of quantum confinement on the three highest valence bands. The second and third highest valence bands are plotted taking the topmost valence band as reference. Here the valence band splitting is lowest for circular wire. Splitting for triangular wire is less

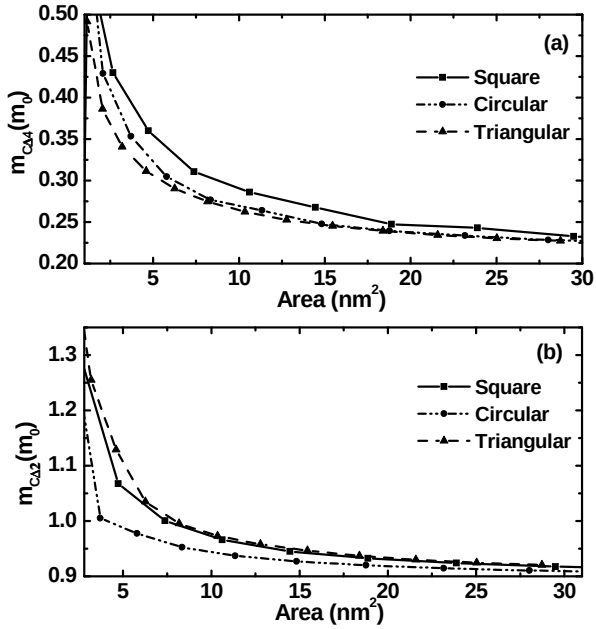

Fig. 6. Electron effective mass for <100> wire at (a) Δ_4 valley (b) Δ_2 valley versus area.

than that of square wire at lower area($< 12.0nm^2$) after which it is similar for both the wires.

Next we calculate effective masses at Δ_4 and Δ_2 valleys for <100> oriented nanowires. The effective mass at Δ_4 valley decreases with wire area and approaches the bulk Si transverse electron effective mass of $0.20^* m_0$ as area is increased as shown in Fig. 6. At Δ_4 valley effective mass is highest for square wire and that of triangular wire is the lowest. m_c^* at Δ_2 valley is lowest for circular wire while that of the other two are almost similar. m_c^* at Δ_2 valley reaches the bulk Si longitudinal electron effective mass of $0.89 m_0^*$ for large wires (>6nm). Electron effective mass at the Γ point for <110> wire m_1 is shown in Fig. 7 (a). With dimension, m_1 increases until it reaches the bulk value ($0.20^* m_0$). Again the triangular wires show lower values than the other two wires. Fig. 7 (b) shows the electron effective mass m_2 at $\pm 0.81 \times \pi/a$. It decreases with wire area and reaches a steady value of $0.55^* m_0$ for large wires. Then we calculate hole effective mass for the highest valence band for <100> wire. Fig. 8 shows the variation of hole effective mass. For triangular wire, hole effective mass is approximately two times larger than that of the bulk Si heavy hole at large dimension. It reaches a value of $-0.5 m_0^*$ for cross-section area $> 20nm^2$. For square and circular wires, hole effective masses are much heavier (atleast five time than the bulk value). m_v^* is highest (magnitude only) for circular wire. For reference, the bulk Si valence band <100> effective mass is $m_{hh} = -0.276 m_0$.

IV. Conclusion

The bandstructure changes silicon nanowires for different cross-section shapes are explored. Most of the electronic properties are different for triangular wire compared to the other two shapes. The bandgap is independent on the wire shape and it only depends on the value of cross-section area. The electron

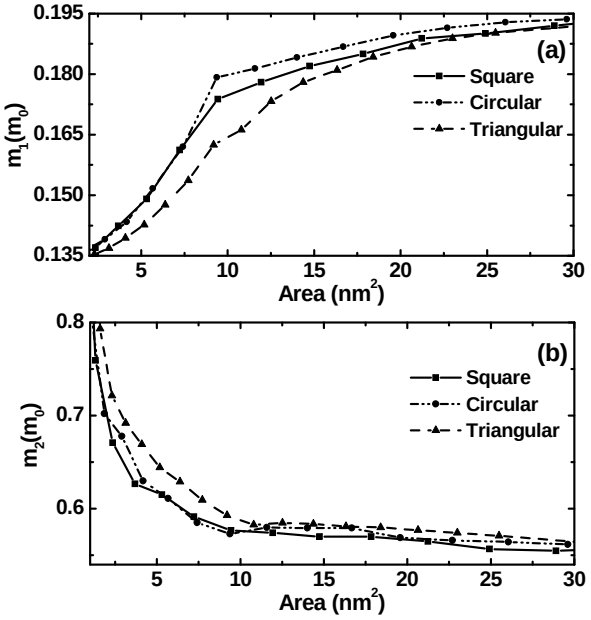

Fig. 7. Variation of electron effective mass with area for <110> wire, (a) m_1 and (b) m_2. The definitions of m_1 and m_2 are given in the text.

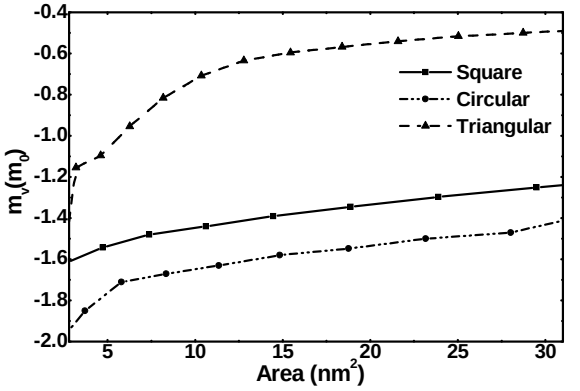

Fig. 8. Variation of hole effective mass with area for <100> wire.

effective mass at the Γ point is lowest for triangular wire for both growth directions (<100> and <110>). The conduction band energies at the Γ point is more degenerate for square and circular wires compared to the triangular wire. And the valence band effective mass for triangular wire is much lower than that for square and circular wires.

ACKNOWLEDGEMENT

The authors would like to thank the Department of Electrical and Electronic Engineering, Bangladesh University of Engineering and Technology for all the simulation facilities.

REFERENCES

[1] Y. Cui, Z. Zhong, D. Wang, W. U. Wang, and C. M. Lieber, "High performance silicon nanowire field effect transistors," Nano Lett., vol. 3, no. 2, pp. 149–152, 2003.

[2] S. M. Koo, M. D. Edelstein, Q. Li, C. A. Richter, and E. M. Vogel, "Silicon nanowires as enhancement-mode Schottky barrier field-effect transistors," Nanotechnology, vol. 16, pp. 1482–1485, 2005.

[3] Y. Huang, X. Duan, Y. Cui, L. J. Lauhon, K. H. Kim, and C. M. Lieber, "Logic gates and computation from assembled nanowire building blocks," Science, vol. 294, pp. 1313–1317, 2001.

[4] Y. Wu, Y. Cui, L. Huynh, C. J. Barrelet, D. C. Bell, and C. M. Lieber, "Controlled growth and structures of molecular-scale silicon nanowires," Nano Lett., vol. 4, no. 3, pp. 433–436, 2004

[5] K. Nehari, N. Cavassilas, J. L. Autran, M. Bescond, D. Munteanu, and M. Lannoo, "Influence of band-structure on electron ballistic transport in silicon nanowire MOSFETs: an atomistic study," Proceedings of ESSDERC, Grenoble, France, 2005, pp. 229 232.

[6] A. Wang, A. Rahman, G. Klimeck, and M. Lundstorm, "Bandstructure and orientation effects in ballistic si and ge nanowire fets," Proceedings of the IEDM. New York: IEEE, 2005, pp. 530533.

[7] Y. Ko, M. Shin, S. Lee, and K. W. Park, "Effects of atomistic defects on coherent electron transmission in si nanowires: full band calculations," J. Appl. Phys., vol. 89, no. 1, pp. 374379, 2001.

[8] E. Durgun, N. Akman, C. Ataca, and S. Ciraci, "Atomic and electronic structures of doped silicon nanowires: A first-principles study," Phys. Rev. B, vol. 76, pp. 245 323/1-8, 2007.

[9] E. Durgun, D. Cakir, N. Akman,and S. Ciraci, "Half-Metallic Silicon Nanowires: First-Principles Calculations," Phys. Rev. Lett., vol. 99, pp. 256 806/1-8, 2007.

[10] T. Vo, A. J. Williamson, and G. Galli, "First principles simulations of the structural and electronic properties of silicon nanowires," Phys. Rev. B, vol. 74, pp. 045 116/1-12, 2006.

[11] M. Shin, "Quantum simulation of device characteristics of silicon nanowire fets," IEEE Transections on Nanotechnology, vol. 6, pp. 230 237, 2007.

[12] J. Wang, A. Rahman, A. Ghosh, G. Klimeck, and M. Lundstrom, "On the validity of the parabolic effective-mass approximation for the i-v calculation of silicon nanowire transistors," IEEE Trans. Electron Dev., vol. 52, no. 7, pp. 1589-95, 2005.

[13] K. Nehari, N. Cavassilas, F. Michelini, M. Bescond, J. L. Autran and M. Lannoo, "Full-band study of current across silicon nanowire transistors," Appl. Phys. Lett., vol. 90, 132112, 2007.

[14] N. Neophytou, A. Paul, M. S.Lundstrom and G. Klimeck, "Simulations of nanowire transistors: atomistic vs. effective mass models," J. of Computational Electronics, vol. 7, no. 3, 2008.

[15] M. Luisier, A. Schenk, and W. Fichtner, "Three-dimensional full-band simulations of Si nanowire transistors," IEDM Tech. Dig., pp. 811815, 2006.

[16] Y. Cui, Z. Zhong, D. Wang, W. U. Wang, C. M. Lieber, "High Performance Silicon Nanowire Field Effect Transistors," Nano Lett., vol. 3, no. 2, pp. 149-152, 2003.

[17] P. Sen, O. Gulseren, T. Yildirim, I. P. Batra, and S. Ciraci, "Pentagonal nanowires: A first-principles study of the atomic and electronic structure," Phys. Rev. B, vol. 65, pp. 235 433/1-7, 2002.

[18] P. B. Sorokin, P. V. Avramov, A. G. Kvashnin, D. G. Kvashnin, S. G. Ovchinnikov, and A. S. Fedorov, "Density functional study of <110>-oriented thin silicon nanowires," Phys. Rev. B, vol. 77, pp. 235 417/1-5, 2008.

[19] T. B. Boykin, G. Klimeck, and F. Oyafuso, "Valence band effective-mass expressions in the $sp^3d^5s^*$ empirical tight-binding model applied to a Si and Ge parametrization," Phys. Rev. B, vol. 69, pp. 115 201/1–10, 2004.

[20] Y. Zheng, C. Rivas, R. Lake, K. Alam, T. B. Boykin, and G. Klimeck, "Electronic properties of silicon nanowires," IEEE Trans. Electron Dev., vol. 52, no. 6, pp. 1097–1103, 2005.

[21] J. C. Slater and G. F. Koster, "Simplified LCAO method for the periodic potential problem," Phys. Rev., vol. 94, no. 6, pp. 1498–1524, 1954.